

---

# Suspected Object Matters: Rethinking Model’s Prediction for One-stage Visual Grounding

---

Yang Jiao<sup>1\*</sup> Zequn Jie<sup>2\*</sup> Jingjing Chen<sup>1</sup> Lin Ma<sup>2</sup> Yu-Gang Jiang<sup>1</sup>

<sup>1</sup>Shanghai Key Lab of Intelligent Information Processing,  
School of Computer Science, Fudan University

<sup>2</sup>Meituan

## Abstract

Recently, one-stage visual grounders attract high attention due to the comparable accuracy but significantly higher efficiency than two-stage grounders. However, inter-object relation modeling has not been well studied for one-stage grounders. Inter-object relationship modeling, though important, is not necessarily performed among all the objects within the image, as only a part of them are related to the text query and may confuse the model. We call these objects “*suspected objects*”. However, exploring relationships among these suspected objects in the one-stage visual grounding paradigm is non-trivial due to two core problems: (1) no object proposals are available as the basis on which to select suspected objects and perform relationship modeling; (2) compared with those irrelevant to the text query, suspected objects are more confusing, as they may share similar semantics, be entangled with certain relationships, etc, and thereby more easily mislead the model’s prediction. To address the above issues, this paper proposes a Suspected Object Graph (SOG) approach to encourage the correct referred object selection among the suspected ones in the one-stage visual grounding. Suspected objects are dynamically selected from a learned activation map as nodes to adapt to the current discrimination ability of the model during training. Afterward, on top of the suspected objects, a Keyword-aware Node Representation module (KNR) and an Exploration by Random Connection strategy (ERC) are concurrently proposed within the SOG to help the model rethink its initial prediction. On the one hand, KNR leverages linguistic keywords contributing high to suspected objects discrimination. On the other hand, ERC allows the model to seek the correct object instead of being trapped in a situation that always exploits the current false prediction. Extensive ablation studies and comparison with state-of-the-art approaches on prevalent visual grounding benchmarks demonstrate the effectiveness of our proposed method.

## 1 Introduction

The Visual Grounding (VG) task [1, 2, 3, 4, 5, 6, 7] aims to detect the specific entity in an image referred by a given referring expression. As such, VG can facilitate users to freely manipulate detection results by the text, which has widespread application prospects in interactive image-editing [8, 9], cross-modal retrieval [10, 11], and so on. The most straightforward approach is a two-stage paradigm [12, 13, 14, 2, 15, 16, 3], where several region proposals are first extracted with an off-the-shelf detector and serve as candidates for the subsequent ranking region-expression pairs. However, such a two-stage paradigm is deficient in two aspects: (i) Region proposals generation brings huge computation cost; (ii) Generated proposals only reflect the confidence of the language

---

\*Equal contribution.



Figure 1: Illustration of (a) text query related objects (inside red boxes) and irrelevant ones (inside blue boxes) according to the given text query; and (b) the activation map generated by a naive one-stage grounder after training five epochs.

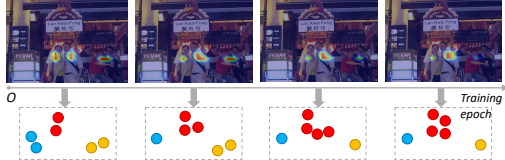


Figure 2: Illustration of the Suspected Object Graph (SOG) nodes evolution process during training, where the nodes gradually converge to the correct object. Please note that the nodes with the same color are located in the same neighborhood in the heat map.

agnostic object detector, thus resulting in missing referred objects. To tackle the above problems, the one-stage visual grounding paradigm [17, 4, 18, 5, 6, 7] has gained great interest in recent years. Motivated by the one-stage detectors [19, 20, 21], one-stage grounding approaches [17, 4] fuses text query embedding with visual features densely at all spatial locations, and directly make the prediction. Such a pipeline gets rid of the heavy region proposal generation in a two-stage pipeline, and thereby avoids valuable regions being filtered [4].

Although effective, these one-stage approaches [17, 4, 6, 7] lack comprehension of relationships between objects, especially those hard to distinguish, which is of vital importance to ground the correct object. For example, as shown in Fig.1(a), investigating relationships among objects inside all labeled bounding boxes is beneficial for building accurate cross-modal correspondence, however, not all objects are worth being equally treated, as only the objects (*i.e.*, men and a woman) inside red bounding boxes are related to the text query “*guy holding the girl*”. We call these objects as “**suspected objects**” in this paper. Compared with other objects, relationships between these suspected objects should be further investigated to identify more distinctive clues for the correct grounding.

Several two-stage methods [14, 15, 3, 16, 22] have studied the inter-object relationship modeling problem. They share the idea of constructing a graph with object proposals denoted as nodes and their relations as edges to benefit learning the correspondence between objects and the referring sentence. Among them, LGRAN [14] considers intra-class and inter-class relationships for edge representations. SGMN [16] makes the fine-grained classification on each edge according to relative distance, relative angle, and Intersection-over-Union of the connected object proposals. Ref-NMS [22] improves the quality of graph nodes by measuring the relevance between each region candidate and the referring sentence when performing the NMS. Though effective enough, such graphs are designed inherently for two-stage methods, requiring object proposals to be extracted as nodes at the first stage. Since the key improvement of the one-stage paradigm lies in getting rid of the problematic region proposal generation process, the graph design in two-stage methods cannot be directly transferred to the one-stage framework [17, 4, 6, 7]. The most straightforward way to realize inter-object communication in the one-stage grounding paradigm is to enlarge the receptive field via conventional non-local [23] operation, deformable convolution [24], etc. Nevertheless, such methods conduct exhaustive message passing for every grid, which is redundant and may even introduce noise from cluttered background and objects irrelevant to the text query, thus hurting the model’s performance as illustrated in Table.3. In this paper, aiming at concise and effective inter-object relationships modeling under the umbrella of one-stage visual grounding, we propose a novel Suspected Object Graph (SOG), which dynamically discovers suspected objects relevant to the text query and gradually disambiguates the referred one from them.

The very first core problem is how to obtain the suspected objects relevant to the text query as graph nodes without the aid of object proposals. Fortunately, we observe that even a naive one-stage grounder can pay high attention to only a limited number of objects after training a few epochs as shown in Fig.1(b)<sup>2</sup>. Hence, suspected objects can be selected according to the one-stage grounder’s initial confidence. It is worth mentioning that unlike the fixed region proposals

<sup>2</sup>More relevant visualization results are included in the supplementary materials.

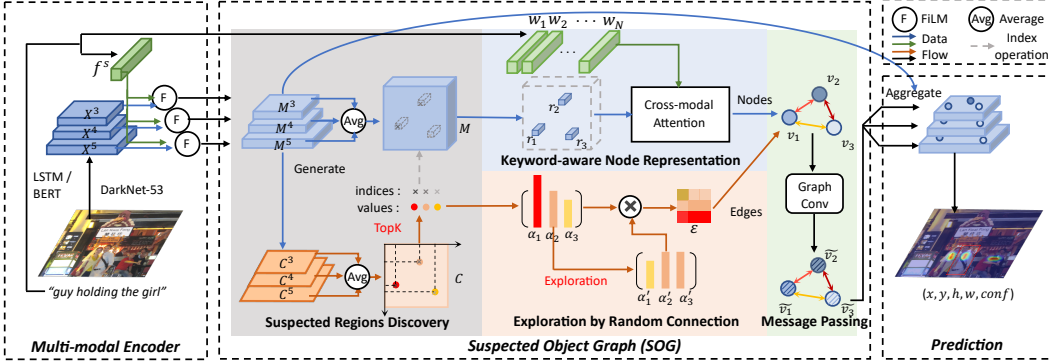


Figure 3: The overall framework of our proposed one-stage grounding method with Suspected Object Graph (SOG), where “ $\otimes$ ” represents the outer product. The visual and textual features are first extracted and interacted in the multi-modal encoder to generate multi-modal features, which are then fed into SOG to select multiple suspected objects. These suspected objects features are served as graph nodes and updated to identify more distinctive clues for distinguishing the referred one from them. Finally, the node features are aggregated with the multi-modal features and make the final prediction. To keep the picture concise, we only illustrate the situation when  $K$  equals 3.

in the two-stage methods [14, 15, 3], the selected suspected objects serving as nodes in SOG can dynamically evolve and finally converge to the correct object during training as illustrated in Fig.2, demonstrating the progressively enhanced suspected object selection ability of the proposed SOG. However, the model’s initial confidence can be unreliable, as these suspected objects are inherently more confusing than others. As shown in Fig.1, they may share similar semantics (several men can correspond to the “*guy*” referred in the expression), entangled within a relationship (the relation “*holding*” binds the guy and girl), etc. Therefore, aiming to help the model rethink its initial selection, we propose a Keyword-aware Node Representation module (KNR) and an Exploration by Random Connection strategy (ERC) within the SOG. On the one hand, KNR leverages linguistic keywords contributing high to suspected objects discrimination. On the other hand, ERC allows the model to seek the correct object instead of being trapped in a situation that always exploits the current false prediction.

In summary, our contributions lie in the following threefold. (1) We explore the inter-object relationships under the umbrella of the one-stage visual grounding framework and propose a Suspected Object Graph (SOG) to disambiguate the referred object from multiple suspected objects. (2) A novel Keyword-aware Node Representation (KNR), as well as an Exploration by Random Connection strategy (ERC) within the SOG, are proposed to facilitate language-guided suspected object discrimination and correct object exploration, respectively. (3) Extensive experimental results on prevalent visual grounding benchmarks demonstrate the effectiveness of our proposed SOG.

## 2 Related Work

### 2.1 Two-stage Visual Grounding.

Enjoying the benefits of several off-the-shelf two-stage object detectors [25, 26], candidate instances in the image are well-extracted, and therefore existing two-stage visual grounding approaches [12, 13, 14, 2, 15, 16, 3] mainly make efforts on devising effective matching mechanism between each candidate and referring expression. In the early years, Hu *et al.* [12] synthesized global context, local descriptor as well as spatial configuration for candidates when scoring with text queries, while Yu *et al.* [13] measures visual differences between multiple candidates. Furthermore, inspired by the success of graph neural networks [27, 28], various works exploit attributes and relationships of objects [14], cross-modal interactions [3], reasoning techniques [15], etc. based on a graph-structured framework. However, the above modeling over-simplifies the composite nature of language into a holistic sentence embedding or a rough subject-predicate object triplet. To this end, Liu [2] *et al.* designs a neural modular tree network to ground each language composite into an image along the

dependency parser tree of the sentence. Similarly, Yang *et al.* [16] parse the sentence into a language scene graph and conduct structured reasoning.

## 2.2 One-stage Visual Grounding.

Recently, the one-stage visual grounding has gained great interest, as it solves two limitations of the two-stage paradigm, *i.e.* the performance cap caused by inaccurate object proposals results, and the long inference time caused by heavy computation in generating object proposals. Instead of extracting all candidate objects in the image, one-stage grounding approaches [17, 4, 18, 5, 6, 7] formulate the whole grounding process in an end-to-end manner. As the pioneer works, SSG [17] and FAQA [4] densely fuse the sentence feature with image features at every locations, and directly make the final prediction. Later, RCCF [18] proposes a cross-modal correlation filter mechanism to select the peak response area as prediction results. Afterward, researchers further make efforts in modeling visual inter-object relations and linguistic contexts. To promote region interactions, the LBYLNet [6] investigates an efficient landmark convolution. Moreover, considering the composite nature of language, ReSC [5] recursively generates sub-queries from sentences to interact with visual features for multiple rounds. Recently, Transformer-based grounder [7] is also proposed for sufficient vision-language communication.

## 3 Methods

The overall framework of our proposed method is shown in Fig.3, where the three components, namely multi-modal encoder, suspected object graph, and prediction are coupled together and can be trained in an end-to-end fashion. Given a paired image and referring expression as input, the multi-modal encoder extracts the visual and textual features and performs cross-modal interactions to generate multi-modal features, which are then fed into our proposed Suspected Object Graph (SOG) to dynamically identify the suspected objects and exploit their relationships. Afterward, the updated node features of SOG, mainly characterizing the suspected objects, are jointly considered with the multi-modal features to make the final grounding prediction.

### 3.1 Multi-modal Encoder

As shown in Fig.3, our proposed model takes an image and a text query as inputs. The sentence feature  $f^s$  and word features  $\{w_n\}_{n=1}^N$  ( $N$  is the sentence length) are extracted with an LSTM [29] or a BERT [30] encoder. Multi-level visual features of the image are extracted with a DarkNet-53 [31] backbone, and then mapped to the same channel dimension using a  $1 \times 1$  convolution. And each level of visual features are concatenated with an 8-D coordinate map to generate position-aware visual features  $X^l \in \mathbb{R}^{h_l \times w_l \times d_m}$ , where  $h_l$  and  $w_l$  are the height and width dimension of  $l$ -th level of visual feature ( $l = \{3, 4, 5\}$  in our implementation). Afterward, FiLM [32] is used to modulate  $X^l$  with the sentence feature  $f^s$  as:

$$\begin{aligned} M^l &= \text{FiLM}(X^l, f^s) \\ &= \text{FC}_\gamma^l(f^s) \odot X^l \oplus \text{FC}_\beta^l(f^s) \end{aligned} \tag{1}$$

where  $\text{FC}_\gamma^l(\cdot)$  and  $\text{FC}_\beta^l(\cdot)$  are two fully-connected layers. “ $\odot$ ” and “ $\oplus$ ” represent element-wise multiplication and addition operation with broadcasting, respectively. Through the FiLM operation, grid features at different locations in multi-modal feature  $M^l$  are adaptively activated as the response to the text query. Different levels of multi-modal features  $M^3, M^4, M^5$  are then served as inputs for SOG.

### 3.2 Suspected Object Graph

As the core component of our method, SOG is responsible for selecting the suspected objects and updating their feature representations, so as to facilitate the model to rethink and gradually correct its selection. As illustrated in Fig.3, the whole SOG consists of four stages. In the first stage, we select several grids with high activation scores based on multi-modal features  $M^3, M^4, M^5$ , and regard them as the suspected regions. Then, these suspected region features as well as their corresponding activation scores are used to construct the SOG nodes and edges, respectively. The

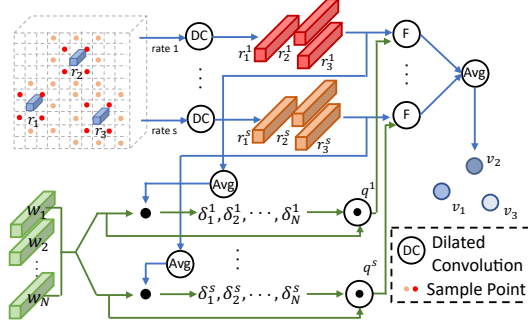


Figure 4: The detailed design of the cross-modal attention module in keyword-aware node representation, where “.” represents the dot product operation, and “ $\odot$ ” stands for the element-wise multiplication with broadcasting.

second and third stages are two independent branches, where the former generates suspected object node representations by leveraging keywords in the text query, and the latter yields edge weights with a novel *exploration by random connection* strategy. Finally, combining with the constructed nodes and edges, we conduct message passing with a standard graph convolution layer.

### 3.2.1 Suspected Regions Discovery.

Considering that no off-the-shelf object candidates are available in one-stage VG, we first identify the regions with suspected objects on which inter-object relationships are expected to be built. Multi-modal feature  $M^l$  shows the relevance to the text query in each visual grid. Hence, to facilitate the subsequent efficient computation, a low dimensional textual activation map  $C^l \in \mathbb{R}^{h_l \times w_l \times 1}$  is produced by dimension reduction with a simple convolution layer:

$$C^l = \text{ReLU}(\text{Conv}(M^l)). \quad (2)$$

To discover suspected objects with different sizes, we integrate  $C^l$  from different scales (*i.e.*,  $C_3, C_4, C_5$ ) to obtain the multi-scale activation map  $\bar{C}$  with average operation. The assembled multi-modal feature  $\bar{M}$  is also generated in a similar way:

$$\bar{M} = \frac{1}{3} \sum_{l=3}^5 M^l, \quad \bar{C} = \frac{1}{3} \sum_{l=3}^5 C^l, \quad (3)$$

where we omit the upsample and downsample operations on  $M^3$  and  $M^5$ .

Based on the obtained multi-modal feature  $\bar{M}$  and activation map  $\bar{C}$ , we choose  $K$  ( $K=6$  in our implementation) grid features from  $\bar{M}$  with the largest intensities in  $\bar{C}$  as the suspected regions. We denote the  $k$ th largest activation score as  $\alpha_k$ , and the corresponding grid feature (*i.e.*, suspected region) as  $r_k$ . By dynamically selecting  $K$  most intensively activated grid features  $\{r_k\}_{k=1}^K$  at each training epoch, the nodes of SOG accordingly evolve along with the training proceeds, such that the model can gradually focus on the most confusing suspected objects to facilitate the correct prediction.

### 3.2.2 Keyword-aware Node Representation.

As illustrated in Fig.1, the suspected objects (*e.g.*, the guy, girl, and sitting man) are usually visually similar and require informative keywords (*e.g.*, holding) in the text query to be further distinguished. Inspired by this, we propose a cross-modal attention module to learn the importance of each word in the referred object discrimination, and assemble word representations weighted by the importance scores to modulate the suspected regions  $r_k$  as shown in Fig.4.

Instead of directly utilizing grid features to interact with word features, we first incorporate context information from the neighboring regions for every suspected region  $r_k$  to effectively learn the representation for objects with different sizes. We apply  $3 \times 3$  dilated convolution [33] with dilation rate  $s$  to aggregate richer object information for every  $r_k$ , and obtain corresponding context-aware

suspected region features  $\{r_k^s\}_{k=1}^K$  accordingly:

$$r_k^s = \sum_u (W_u g_u), \quad \forall u \in \mathcal{N}^s(r_k), \quad (4)$$

where  $\mathcal{N}^s(r_k)$  is the neighborhood of  $r_k$  (including the  $r_k$ ) when dilation rate is  $s$ , and  $g_u$  is a grid feature in this neighborhood. Afterward,  $\{r_k^s\}_{k=1}^K$  are averaged and matched with every word feature  $w_n$  to generate the importance score  $\delta_n^s$ :

$$\begin{aligned} \bar{r}^s &= \frac{1}{K} \sum_{k=1}^K r_k^s, \\ \delta_n^s &= \frac{\exp(\bar{r}^s \cdot w_n)}{\sum_{m=1}^N \exp(\bar{r}^s \cdot w_m)}, \end{aligned} \quad (5)$$

where “.” denotes the dot product. Then we calculate a keyword-aware textual representation  $q^s$  with a weighted combination of word features, where the word with higher importance score  $\delta_n^s$  contributes more in constructing  $q^s$ . Next, the region feature  $r_k^s$  is first modulated by the keyword-aware textual representation  $q^s$  with the FiLM module, and then aggregated to generate corresponding suspected object feature  $v_k$ , which also serves as the node in SOG. The above operations can be formulated as:

$$\begin{aligned} q^s &= \sum_{n=1}^N \delta_n^s \odot w_n, \\ v_k &= \frac{1}{|\mathcal{S}|} \sum_s \text{FiLM}(r_k^s, q^s), \quad \forall s \in \mathcal{S}, \end{aligned} \quad (6)$$

where  $\mathcal{S}$  is the collection of values for the dilation rate ( $\mathcal{S}=\{1, 6, 12\}$  in our implementation). We denote the SOG nodes as  $\mathcal{V} = \{v_k\}_{k=1}^K$ .

### 3.2.3 Exploration by Random Connection.

With  $K$  activation scores  $\{\alpha_k\}_{k=1}^K$  as inputs, a straightforward way to generate the edge weight  $e_{ij}$  from node  $v_i$  to node  $v_j$  can be defined as:

$$e_{ij} = \alpha_i \odot \alpha_j. \quad (7)$$

Message passing can be performed among the suspected objects which are the nodes in the SOG through the above connection weights, to achieve the inter-object relationship modeling. However, the above edge construction strategy imposes high connection strength between the nodes with high activation scores. In this way, an incorrect object with high activation would have a higher impact after feature integration via message passing in SOG. Hence, if the initial incorrect objects obtain high activation scores, the model is easily trapped in a situation that always exploits the current false object selection as shown in Fig.5 (a), deviating from the goal of the object selection rethinking and correction.

To balance between trusting the model’s initial judgement and preventing the aforementioned error remaining problem, we propose an *exploration by random connection* strategy to moderately decouple the edge strength from node activation. Specifically, motivated by the data augmentation technique in BERT [30] that replaces a certain token with another random token 10% of the time, we remain  $\alpha_k$  unchanged with the probability  $p$  ( $p = 0.5$  in our implementation), and uniformly sample a substitution from other  $\alpha$  values. We denote  $\alpha'_k$  as the result of  $\alpha_k$  processed with exploration by random connection, and  $e_{ij}$  can be reformulated by replacing  $\alpha_j$  with  $\alpha'_j$  in Eq.(7) accordingly:

$$e_{ij} = \alpha_i \odot \alpha'_j. \quad (8)$$

As such, SOG edges are obtained, which is formulated as  $\mathcal{E} = \{e_{ij}\}_{i,j=1}^K$ .

### 3.2.4 Message Passing.

So far, both the nodes  $\mathcal{V}$  and edges  $\mathcal{E}$  of SOG have been constructed. We conduct conventional graph convolution to update node representations by aggregating the features of the neighboring connected nodes:

$$\tilde{v}_k = \sum_{j \in \{1, 2, \dots, K\}} e_{jk} \odot v_j, \quad (9)$$

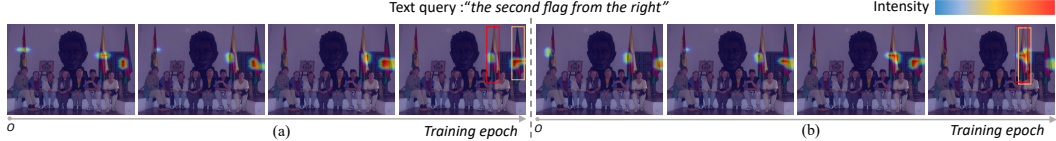


Figure 5: The influence of our proposed exploration by random connection strategy (ERC) to SOG graph nodes evolution process. The red and orange bounding boxes represent the ground-truth and model prediction results, respectively. (a) Without the ERC, the previous false judgement is passed on and accumulated with training proceeds, demonstrating the error remaining problem. (b) With the ERC, edge weights are decoupled from model judgement confidence, and therefore prevent the wrong judgement from affecting the later decision, which finally yields the correct grounding results.

where  $\tilde{v}_k$  is the updated graph node representation.

Our SOG gradually evolves by dynamically adjusting its suspected object graph nodes (selecting the  $K$  grid features with the largest response in the activation map) during training. And the message passing among these graph nodes (suspected objects) achieves the goal of inter-object relationship modeling. As such, during each training epoch, our proposed SOG can rethink the identified suspected objects and thereafter correct its choice for suspected objects in the next training epoch.

### 3.3 Prediction

Carrying more distinctive clues of referred object, the updated node features  $\{\tilde{v}_k\}_{k=1}^K$  together with the multi-modal features  $M^3, M^4$  and  $M^5$  are aggregated and fed into a prediction head for grounding the referred object. Specifically, a typical prediction head first generates an output with the dimension of  $h_l \times w_l \times 3 \times 5$ , where 3 is the number of anchors set at each grid and 5 is for several 5-D tuples like  $(t_x, t_y, t_h, t_w, conf)$ , where the first four values are the bounding box offsets relative to the pre-defined anchors and the last one is the confidence of including the referred object at this position.

### 3.4 Training and Inference

Following the previous methods [4, 5, 6], we apply a cross-entropy loss  $\mathcal{L}_{conf}$  on the confidence score  $conf$  and a MSE loss  $\mathcal{L}_{off}$  on the coordinate offsets  $t_x, t_y, t_h, t_w$  for each grid. The whole loss function for training our proposed model is denoted as:

$$\mathcal{L} = \mathcal{L}_{conf} + \lambda_{off} * \mathcal{L}_{off}, \quad (10)$$

where  $\lambda_{off} = 5$  is the coefficients empirically set to balance loss terms.

During inference, a paired image and referring expression are taken as the input of our model, with the predicted bounding box of the highest confidence score being regarded as the final prediction result.

## 4 Experiments

### 4.1 Experimental Setup

**Datasets.** We conduct experiments on four benchmark datasets, namely ReferIt [40], RefCOCO [13], RefCOCO+ [13] and RefCOCOg [41]. Referred entities in ReferIt are selected from SAIAPR-12 dataset [42], where the entities can be objects or stuff (e.g., sky). There are 54,127/ 5,842/ 60,103 referring expressions in “train”/ “validation”/ “test” set respectively. For RefCOCO [13], RefCOCO+ [13] and RefCOCOg [41], the objects are selected from MSCOCO [43], hence in total there are which 80 object categories. Both RefCOCO and RefCOCO+ are splitted into “train”, “validation”, “testA” and “testB” set following [13]. Referred objects in “testA” are people, while those in “testB” are objects of other categories. “Train”/ “validation”/ “testA”/ “testB” has 120,624/ 10,834/ 5,657/ 5,095 referring expressions for RefCOCO, and 120,191/ 10,758/ 5,726/ 4,889 referring expressions for RefCOCO+. No position pointing words (e.g., “left”, “right”) appeared in RefCOCO+, which increases the difficulty of locating the target object.

Table 1: Comparison with state-of-the-art methods on RefCOCO, RefCOCO+, RefCOCOg. “R-101”, “R-50” and “D-53” represent “ResNet-101”, “ResNet-50” and “DarkNet-53”, respectively. In two stage methods, we use \* to indicate that this model uses ground-truth bounding boxes as input. The best performances in two-stage methods (except the DGA\* for fair comparison) are highlighted with underline, and the best performances in transformer-based and CNN-based one-stage methods are highlighted with ***bold italics*** and ***bold***, respectively.

| Methods                  | Visual & Text Encoder | Image size | RefCOCO      |              |              | RefCOCO+     |              |              | RefCOCOg val | Time (ms) |
|--------------------------|-----------------------|------------|--------------|--------------|--------------|--------------|--------------|--------------|--------------|-----------|
|                          |                       |            | val          | testA        | testB        | val          | testA        | testB        |              |           |
| <i>Two-stage methods</i> |                       |            |              |              |              |              |              |              |              |           |
| CMN [34]                 | VGG16 & LSTM          | -          | -            | 71.03        | 65.77        | -            | 54.32        | 47.76        | -            | -         |
| VC [35]                  | VGG16 & LSTM          | -          | -            | 73.33        | 67.44        | -            | 50.86        | 58.03        | -            | -         |
| ParallelAttn [36]        | VGG16 & LSTM          | -          | -            | 75.31        | 65.52        | -            | 61.34        | 50.86        | -            | -         |
| LGRAN [14]               | VGG16 & LSTM          | -          | -            | 76.6         | 66.4         | -            | 64.00        | 53.40        | 61.78        | -         |
| SLR [37]                 | R-101 & LSTM          | -          | 69.48        | 73.71        | 64.96        | 55.71        | 60.74        | 48.80        | -            | -         |
| MAttNet [38]             | R-101 & LSTM          | -          | 76.40        | 80.43        | 69.28        | 64.93        | 70.26        | 56.00        | -            | 320       |
| DGA [15]                 | R-101 & LSTM          | -          | -            | 78.42        | 65.53        | -            | 69.07        | 51.99        | -            | 341       |
| DGA* [15]                | R-101 & LSTM          | -          | 86.34        | 86.64        | 84.79        | 73.56        | 78.31        | 68.15        | 80.21        | 341       |
| CM-A-E [39]              | R-101 & LSTM          | -          | 78.35        | 83.14        | 71.32        | 68.09        | 73.65        | 58.03        | 68.67        | -         |
| CM-A-E+Ref-NMS [22]      | R-101 & LSTM          | -          | <b>80.70</b> | <b>84.00</b> | <b>76.04</b> | <b>68.25</b> | <b>73.68</b> | <b>59.42</b> | <b>70.62</b> | -         |
| NMTree [2]               | R-101 & T-LSTM        | -          | 76.41        | 81.21        | 70.09        | 66.46        | 72.02        | 57.52        | 64.62        | -         |
| <i>One-stage methods</i> |                       |            |              |              |              |              |              |              |              |           |
| <i>Transformer-based</i> |                       |            |              |              |              |              |              |              |              |           |
| TransVG [7]              | R-50 & BERT           | 640×640    | 80.32        | 82.67        | 78.12        | 63.50        | 68.15        | 55.63        | 66.56        | 61.77     |
| TransVG [7]              | R-101 & BERT          | 640×640    | <b>81.02</b> | <b>82.72</b> | <b>78.35</b> | <b>64.82</b> | <b>70.70</b> | <b>56.94</b> | <b>67.02</b> | -         |
| <i>CNN-based</i>         |                       |            |              |              |              |              |              |              |              |           |
| SSG [17]                 | D-53 & LSTM           | 416×416    | -            | 76.51        | 67.50        | -            | 62.14        | 49.27        | 47.47        | 25        |
| FAQA [4]                 | D-53 & BERT           | 256×256    | 72.54        | 74.35        | 68.50        | 56.81        | 60.23        | 49.60        | 56.12        | 23        |
| RCCF [18]                | DLA-34 & LSTM         | 512×512    | -            | 81.06        | 71.85        | -            | 70.35        | 56.32        | -            | 25        |
| ReSC-Large [5]           | D-53 & BERT           | 256×256    | 77.63        | 80.45        | 72.30        | 63.59        | 68.36        | 56.81        | 63.12        | 36        |
| LBYLNet [6]              | D-53 & BERT           | 256×256    | 79.67        | 82.91        | 74.15        | 68.64        | 73.38        | 59.49        | 62.70        | 30        |
| SOG(Ours)                | D-53 & BERT           | 256×256    | 81.35        | 82.82        | 77.35        | 68.65        | 73.80        | 61.18        | 63.87        | 31        |
| SOG(Ours)                | D-53 & BERT           | 416×416    | <b>82.11</b> | <b>83.79</b> | <b>78.14</b> | <b>70.89</b> | <b>75.81</b> | <b>62.75</b> | <b>65.29</b> | 39        |

**Implementation details.** DarkNet-53 pre-trained on MSCOCO is used as the image encoder, and LSTM or BERT [44] is used as the text encoder. Since previous one-stage VG methods [17, 4, 18, 7] adopt different input resolutions, we resize input image size to 256×256 and 416×416 to evaluate the performances under different resolutions. Experiments are conducted with input resolution 256×256 unless specified. The Adam [45] optimizer with an initial learning rate of  $1e^{-4}$ , weight decay of  $1e^{-4}$ , and batch size of 64 is used to train our network. The learning rate is decreased with a cosine annealing strategy [46]. Following previous work [6], we train our network 100 epochs on ReferIt, RefCOCO and RefCOCO+, and 30 epochs on RefCOCOg. During the evaluation, we deactivate our proposed exploration by random connection strategy to eliminate randomness. Following prior works [4, 5, 6],  $Pr@0.5(\%)$  is adopted as the evaluation metric. All the experiments are conducted on the Geforce-GTX-1080Ti GPU and CUDA 10.2 with Intel(R) Xeon(R) CPU E5-2640 v4 @ 2.40GHz.

## 4.2 Comparison with State-of-the-art Methods

We compare our proposed method with state-of-the-art approaches on RefCOCO, RefCOCO+, RefCOCOg and ReferIt in Table 1 and Table 2. For a more convenient comparison, we group existing methods into two-stage methods and one-stage methods, respectively. Besides, one-stage methods can be further split into CNN-based and Transformer-based methods. For fair comparisons, different encoders and different image resolutions are considered.

Table 1 lists the results on COCO series datasets (*i.e.*, RefCOCO, RefCOCO+, RefCOCOg). From the results, we have the following observations. First, our method outperforms existing CNN-based one-stage methods in most cases. When using BERT as text encoder, our method obtain 1.67%, 3.2% and 1.69% improvements on the RefCOCO val, testB set and RefCOCO+ testB set over the strongest CNN-based competitor LBYLNet [6]. Second, our method also achieves competitive performances when comparing with the transformer-based method TransVG [7] even using a lower resolution input (416×416 vs 640×640). On RefCOCO+, our method even outperforms TransVG with a large margin. It is worthwhile mentioning that the inference speed of our method is much faster than

<sup>3</sup>“mix” means firstly train the model on the image that resized to 300×300 and then retrain the model on images with the size of 600×600.

Table 2: Comparison with state-of-the-art methods on ReferIt.

| Methods                  | Visual & Text Encoder | Input size       | ReferIt test | Time (ms) |
|--------------------------|-----------------------|------------------|--------------|-----------|
| <i>Two-stage Methods</i> |                       |                  |              |           |
| CMN [34]                 | VGG16 & LSTM          | -                | 28.33        | -         |
| VC [35]                  | VGG16 & LSTM          | -                | 31.13        | -         |
| MAttNet [38]             | R-101 & LSTM          | -                | 29.04        | 184       |
| Similarity Net [47]      | R-101 & -             | -                | 34.54        | 196       |
| CITE [48]                | R-101 & -             | -                | 35.07        | 320       |
| DDPN [1]                 | R-101 & LSTM          | -                | 63.00        | -         |
| <i>One-stage Methods</i> |                       |                  |              |           |
| <i>Transformer-based</i> |                       |                  |              |           |
| TransVG [7]              | R-50 & BERT           | 640×640          | 69.76        | 61.77     |
| TransVG [7]              | R-101 & BERT          | 640×640          | <b>70.73</b> | -         |
| <i>CNN-based</i>         |                       |                  |              |           |
| SSG [17]                 | D-53 & LSTM           | 416×416          | 54.24        | 25        |
| ZSGNet [49]              | R-50 & LSTM           | mix <sup>3</sup> | 58.63        | 25        |
| FAQA [4]                 | D-53 & BERT           | 256×256          | 60.67        | 23        |
| RCCF [18]                | DLA-34 & LSTM         | 512×512          | 63.79        | 25        |
| ReSC-Large [5]           | D-53 & BERT           | 256×256          | 64.60        | 36        |
| LBYLNet [6]              | D-53 & BERT           | 256×256          | 67.47        | 30        |
| SOG(Ours)                | D-53 & BERT           | 256×256          | 68.57        | 31        |
| SOG(Ours)                | D-53 & BERT           | 416×416          | <b>69.50</b> | 39        |

Table 3: Performance comparison of context modeling graphs with different nodes formats in the one-stage VG on ReferIt dataset.

| Model               | Graph Nodes Formats for Context Modeling | Pr@0.5 (%)   |
|---------------------|--|--------------|
| <i>Baseline</i>     | -  | 62.47        |
| <i>+Nonlocal</i>    | <i>dense grids</i>                       | 64.03        |
| <i>+Deform Conv</i> | <i>dense grids</i>                       | 64.42        |
| <i>+SOG</i>         | <i>suspected objects</i>                 | <b>66.11</b> |

Table 4: Performance comparison with and without KNR or ERC on ReferIt dataset. “w/o ERC” means calculating edge weights with Eq.(7).

| Nodes Construction w/o KNR | Nodes Construction w/ KNR | Edges Construction w/o ERC | Edges Construction w/ ERC | Pr@0.5 (%)   |
|----------------------------|---------------------------|----------------------------|---------------------------|--------------|
| ✓                          |                           | ✓                          |                           | 64.48        |
| ✓                          |                           |                            | ✓                         | 64.99        |
|                            | ✓                         | ✓                          |                           | 65.53        |
|                            | ✓                         | ✓                          | ✓                         | <b>66.11</b> |

TransVG. Third, our method performs better than all of the two-stage methods on both RefCOCO and RefCOCO+ datasets. However, on RefCOCOg, our proposed method is inferior to the two-stage method CM-A-E [39]. This is mainly due to that the text queries in RefCOCOg are longer than those in other datasets, which are not comprehensively modeled by our method. In contrast, both CM-A-E and TransVG are designed to deal with long texts by mining the complex correspondence between objects and each word, hence achieving better performances. Finally, as two ways to improve the quality of proposals in the two-stage paradigm, Ref-NMS [22] (CM-A-E+Ref-NMS) and DGA\* that directly uses ground-truth bounding boxes brought evident improvements compared with their corresponding baselines (i.e., CM-A-E and DGA in respectively). This further demonstrates that the bottleneck of two-stage paradigm is that valuable proposals are filtered by the region proposal process as claimed in the Sec.1.

Table 2 summarizes the performance comparisons on the ReferIt dataset. Generally, most of two-stage methods perform poorly on this dataset. This might be due to the poor candidate object detection results, since their detectors in the first stage are pre-trained on MSCOCO. As a result, no qualified candidate objects are available for matching with text queries. By getting rid of candidate object detection, one-stage methods, perform much better than most of the two-stage methods. Overall, our method achieves competitive performances compared to the state-of-the-art transformer-based one-stage method, despite that the resolution of the input image in our method is smaller.

### 4.3 Ablation Studies

We first conduct ablation studies on ReferIt dataset to verify the effectiveness of different modules in our framework, including sparse Suspected Object Graph (SOG) for context modeling, Keyword-aware Node Representation (KNR) and Exploration by Random Connection (ERC) for constructing nodes and edges in SOG. Here LSTM is used as the text encoder, and all models are trained with the same strategy described before for fair comparisons.

Table 5: Performances of alternative strategies of ERC.

| Strategy         | Pr@0.5(%)    |
|------------------|--------------|
| <i>original</i>  | 65.53        |
| <i>reverse</i>   | 65.41        |
| <i>average</i>   | 65.73        |
| <i>random</i>    | 65.57        |
| <i>ERC(Ours)</i> | <b>66.11</b> |

Table 6: Performances of alternative strategies of KNR.

| Strategy            | Pr@0.5(%)    |
|---------------------|--------------|
| -                   | 64.99        |
| <i>sentence</i>     | 64.61        |
| <i>word average</i> | 64.45        |
| <i>KNR(Ours)</i>    | <b>66.11</b> |

**Dense grids vs. sparse suspected objects.** Table 3 compares the proposed SOG against the basic one-stage grounder equipped with a non-local block [23] and a deformable convolution layer [24], two representative approaches to conduct exhaustive message passing among all grids. In the table, the *Baseline* is implemented by combining “Multi-modal Encoder” with “Prediction” presented in Fig.3, hence no visual inter-object relationship modeling is applied for the baseline. For fair comparisons, we include a standard nonlocal block and a deformable convolution layer on dense grids for visual inter-object relationship modeling. From the results, we have the following observations. First, our SOG with selected sparse suspected objects performs much better than the baseline equipped with a dense grids modeling layer (*i.e.*, with a nonlocal block and a deformable convolution layer), showing the advantages of reasoning on a few suspected objects for visual grounding. This is mainly due to that SOG helps reduce the noise introduced by irrelevant regions. Second, compared to the baseline, adding either a dense grids modeling layer or our proposed SOG could achieve much better performances, which demonstrates the importance of inter-object relationship modeling.

**Effectiveness of KNR and ERC.** We further verify the effectiveness of our KNR and ERC in Table 4. From the results, KNR and ERC improve the base model 0.51% and 1.05%, respectively. By applying both KNR and ERC on the base model, the performance can be further improved to 66.11%. The results demonstrate the effectiveness of our proposed KNR and ERC in distinguishing the referred object from multiple suspected objects.

#### 4.4 Alternative Strategies for ERC and KNR.

To further verify the effectiveness of our proposed ERC and KNR, we demonstrate some other possible strategies for replacing them in Table 5 and Table 6.

**ERC.** As for the ERC, there are some alternatives to calculate  $\alpha'_j$  in Eq.(8) as listed below: **(1) original:**  $\alpha'_j = \alpha_j$  **(2) reverse:**  $\alpha'_j = \alpha_{K-j+1}$  **(3) average:**  $\alpha'_j = \frac{1}{K} \sum_{k=1}^K \alpha_k$  **(4) random:**  $\alpha'_j \sim \mathcal{N}(0, 1)$

Compared with other strategies, our proposed ERC not only complies with model’s initial choice (*i.e.*, keeping  $\alpha'_j = \alpha_j$  with probability  $p$ ), but also has chances to break up the dependencies between edge weights and model confidence (*i.e.*, assigning  $\alpha'_j$  with a value uniformly sampled from  $\{\alpha_k\}_{k \in \{1, \dots, K\} \setminus \{j\}}$  with probability  $1-p$ ). With the above merits, our ERC achieves 0.58% performance improvement compared with the baseline (*i.e.*, *original*) without introducing extra computation.

**KNR.** As for the KNR, we design two counterparts (*i.e.*, *sentence* and *word average*) as shown in Table 6, where the suspected node features are modulated by sentence-level feature from LSTM and averaged words feature, respectively. “-” in the first row means no language information is used to modulate nodes. We observe that simply using sentence feature or the averaged words feature even degenerates the model, as they introduce too much noise from the irrelevant words. By excavating keywords, our KNR can bring 1.12% absolute improvements on ReferIt test set.

#### 4.5 Qualitative Results

Fig.6 visualizes words’ attention in KNR and the nodes’ attention in the final SOG graph. A higher words attention means a larger contribution in suspected objects, *e.g.*, “suit” in Fig.6 (a). As can be seen, the nodes in our SOG graph converge to the referred objects. Fig.7 further shows the SOG nodes’ attention changes during the training process. In the early training epochs, a confusing object (*e.g.*, the front man in blue in the second example) gains more attention, while another one (*e.g.*, the woman sitting behind) easy to be discriminated is seldom selected as nodes. With training continuing,

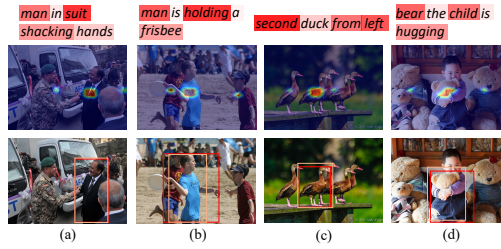


Figure 6: Qualitative results of our proposed SOG (best viewed in color). The darker background color of the word represents the higher attention to it, and the heat maps are generated by mapping SOG nodes activation into the original image. Orange and red boxes are the prediction results and ground-truths, respectively.

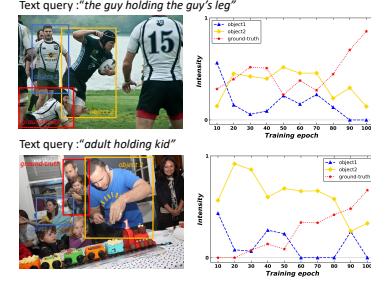


Figure 7: The evolution of SOG nodes' attention in training. We manually label the bounding boxes of some suspected objects, and sum the activation scores of the nodes falling inside each bounding box as SOG nodes' attention to it.

SOG nodes' attention gradually shifts from the confusing object to the ground-truth object. More qualitative results can be found in supplementary materials.

## 5 Conclusions

In this paper, we focused on the relation modeling of suspected objects in the one-stage visual grounding and proposed a Suspected Object Graph (SOG). By adaptively selecting suspected objects as nodes during training, our SOG could filter cluttered background and focus on discriminating the target objects from multiple suspected ones. Besides, to deal with the wrong suspected object selection problem, we designed two strategies, Keyword-aware Node Representation (KNR) and Exploration by Random Connection (ERC). With the help of our proposed KNR and ERC, the selected nodes of SOG could gradually evolve and finally converge to the correct object with training proceeds. Extensive experimental results proved the effectiveness of our proposed method.

## References

- [1] Zhou Yu, Jun Yu, Chenchao Xiang, Zhou Zhao, Qi Tian, and Dacheng Tao. Rethinking diversified and discriminative proposal generation for visual grounding. In Jérôme Lang, editor, *Proceedings of the Twenty-Seventh International Joint Conference on Artificial Intelligence, IJCAI 2018, July 13-19, 2018, Stockholm, Sweden*, pages 1114–1120. ijcai.org, 2018.
- [2] Daqing Liu, Hanwang Zhang, Zheng-Jun Zha, and Feng Wu. Learning to assemble neural module tree networks for visual grounding. In *2019 IEEE/CVF International Conference on Computer Vision, ICCV 2019, Seoul, Korea (South), October 27 - November 2, 2019*, pages 4672–4681. IEEE, 2019.
- [3] Yongfei Liu, Bo Wan, Xiaodan Zhu, and Xuming He. Learning cross-modal context graph for visual grounding. In *The Thirty-Fourth AAAI Conference on Artificial Intelligence, AAAI 2020, The Thirty-Second Innovative Applications of Artificial Intelligence Conference, IAAI 2020, The Tenth AAAI Symposium on Educational Advances in Artificial Intelligence, EAAI 2020, New York, NY, USA, February 7-12, 2020*, pages 11645–11652. AAAI Press, 2020.
- [4] Zhengyuan Yang, Boqing Gong, Liwei Wang, Wenbing Huang, Dong Yu, and Jiebo Luo. A fast and accurate one-stage approach to visual grounding. In *ICCV*, 2019.
- [5] Zhengyuan Yang, Tianlang Chen, Liwei Wang, and Jiebo Luo. Improving one-stage visual grounding by recursive sub-query construction. In *ECCV*, 2020.
- [6] Binbin Huang, Dongze Lian, Weixin Luo, and Shenghua Gao. Look before you leap: Learning landmark features for one-stage visual grounding. In *IEEE/CVF Conference on Computer Vision and Pattern Recognition (CVPR)*, June 2021.
- [7] Jiajun Deng, Zhengyuan Yang, Tianlang Chen, Wengang Zhou, and Houqiang Li. Transvg: End-to-end visual grounding with transformers. *arXiv preprint arXiv:2104.08541*, 2021.
- [8] Brian L. Price and William A. Barrett. Object-based vectorization for interactive image editing. *Vis. Comput.*, 22(9-11):661–670, 2006.
- [9] Erik Conser, Kennedy Hahn, Chandler M. Watson, and Melanie Mitchell. Revisiting visual grounding. *CoRR*, abs/1904.02225, 2019.
- [10] Xue Song, Jingjing Chen, Zuxuan Wu, and Yu-Gang Jiang. Spatial-temporal graphs for cross-modal text2video retrieval. *IEEE Transactions on Multimedia*, 2021.
- [11] Bin Zhu, Chong-Wah Ngo, Jingjing Chen, and Yanbin Hao. R2GAN: cross-modal recipe retrieval with generative adversarial network. In *IEEE Conference on Computer Vision and Pattern Recognition, CVPR 2019, Long Beach, CA, USA, June 16-20, 2019*, pages 11477–11486. Computer Vision Foundation / IEEE, 2019.
- [12] Ronghang Hu, Huazhe Xu, Marcus Rohrbach, Jiashi Feng, Kate Saenko, and Trevor Darrell. Natural language object retrieval. In *2016 IEEE Conference on Computer Vision and Pattern Recognition, CVPR 2016, Las Vegas, NV, USA, June 27-30, 2016*, pages 4555–4564. IEEE Computer Society, 2016.
- [13] Licheng Yu, Patrick Poirson, Shan Yang, Alexander C. Berg, and Tamara L. Berg. Modeling context in referring expressions. In Bastian Leibe, Jiri Matas, Nicu Sebe, and Max Welling, editors, *Computer Vision - ECCV 2016 - 14th European Conference, Amsterdam, The Netherlands, October 11-14, 2016, Proceedings, Part II*, volume 9906 of *Lecture Notes in Computer Science*, pages 69–85. Springer, 2016.
- [14] Peng Wang, Qi Wu, Jiewei Cao, Chunhua Shen, Lianli Gao, and Anton van den Hengel. Neighbourhood watch: Referring expression comprehension via language-guided graph attention networks. In *IEEE Conference on Computer Vision and Pattern Recognition, CVPR 2019, Long Beach, CA, USA, June 16-20, 2019*, pages 1960–1968. Computer Vision Foundation / IEEE, 2019.
- [15] Sibei Yang, Guanbin Li, and Yizhou Yu. Dynamic graph attention for referring expression comprehension. In *2019 IEEE/CVF International Conference on Computer Vision, ICCV 2019, Seoul, Korea (South), October 27 - November 2, 2019*, pages 4643–4652. IEEE, 2019.
- [16] Sibei Yang, Guanbin Li, and Yizhou Yu. Graph-structured referring expression reasoning in the wild. In *Proceedings of the IEEE Conference on Computer Vision and Pattern Recognition*, 2020.

- [17] Xinpeng Chen, Lin Ma, Jingyuan Chen, Zequn Jie, Wei Liu, and Jiebo Luo. Real-time referring expression comprehension by single-stage grounding network. *CoRR*, abs/1812.03426, 2018.
- [18] Yue Liao, Si Liu, Guanbin Li, Fei Wang, Yanjie Chen, Chen Qian, and Bo Li. A real-time cross-modality correlation filtering method for referring expression comprehension. In *2020 IEEE/CVF Conference on Computer Vision and Pattern Recognition, CVPR 2020, Seattle, WA, USA, June 13-19, 2020*, pages 10877–10886. Computer Vision Foundation / IEEE, 2020.
- [19] Joseph Redmon, Santosh Kumar Divvala, Ross B. Girshick, and Ali Farhadi. You only look once: Unified, real-time object detection. In *2016 IEEE Conference on Computer Vision and Pattern Recognition, CVPR 2016, Las Vegas, NV, USA, June 27-30, 2016*, pages 779–788. IEEE Computer Society, 2016.
- [20] Wei Liu, Dragomir Anguelov, Dumitru Erhan, Christian Szegedy, Scott E. Reed, Cheng-Yang Fu, and Alexander C. Berg. SSD: single shot multibox detector. In Bastian Leibe, Jiri Matas, Nicu Sebe, and Max Welling, editors, *Computer Vision - ECCV 2016 - 14th European Conference, Amsterdam, The Netherlands, October 11-14, 2016, Proceedings, Part I*, volume 9905 of *Lecture Notes in Computer Science*, pages 21–37. Springer, 2016.
- [21] Zhi Tian, Chunhua Shen, Hao Chen, and Tong He. FCOS: fully convolutional one-stage object detection. In *2019 IEEE/CVF International Conference on Computer Vision, ICCV 2019, Seoul, Korea (South), October 27 - November 2, 2019*, pages 9626–9635. IEEE, 2019.
- [22] Long Chen, Wenbo Ma, Jun Xiao, Hanwang Zhang, and Shih-Fu Chang. Ref-nms: Breaking proposal bottlenecks in two-stage referring expression grounding. In *Proceedings of the AAAI Conference on Artificial Intelligence*, number 2, pages 1036–1044, 2021.
- [23] Xiaolong Wang, Ross B. Girshick, Abhinav Gupta, and Kaiming He. Non-local neural networks. In *2018 IEEE Conference on Computer Vision and Pattern Recognition, CVPR 2018, Salt Lake City, UT, USA, June 18-22, 2018*, pages 7794–7803. Computer Vision Foundation / IEEE Computer Society, 2018.
- [24] Jifeng Dai, Haozhi Qi, Yuwen Xiong, Yi Li, Guodong Zhang, Han Hu, and Yichen Wei. Deformable convolutional networks. In *IEEE International Conference on Computer Vision, ICCV 2017, Venice, Italy, October 22-29, 2017*, pages 764–773. IEEE Computer Society, 2017.
- [25] Shaoqing Ren, Kaiming He, Ross Girshick, and Jian Sun. Faster r-cnn: Towards real-time object detection with region proposal networks. *Advances in neural information processing systems*, 28:91–99, 2015.
- [26] Kaiming He, Georgia Gkioxari, Piotr Dollár, and Ross B. Girshick. Mask R-CNN. In *IEEE International Conference on Computer Vision, ICCV 2017, Venice, Italy, October 22-29, 2017*, pages 2980–2988. IEEE Computer Society, 2017.
- [27] Thomas N. Kipf and Max Welling. Semi-supervised classification with graph convolutional networks. In *5th International Conference on Learning Representations, ICLR 2017, Toulon, France, April 24-26, 2017, Conference Track Proceedings*. OpenReview.net, 2017.
- [28] Petar Velickovic, Guillem Cucurull, Arantxa Casanova, Adriana Romero, Pietro Liò, and Yoshua Bengio. Graph attention networks. *CoRR*, abs/1710.10903, 2017.
- [29] Sepp Hochreiter and Jürgen Schmidhuber. Long short-term memory. *Neural computation*, 9(8):1735–1780, 1997.
- [30] Jacob Devlin, Ming-Wei Chang, Kenton Lee, and Kristina Toutanova. BERT: pre-training of deep bidirectional transformers for language understanding. In Jill Burstein, Christy Doran, and Thamar Solorio, editors, *Proceedings of the 2019 Conference of the North American Chapter of the Association for Computational Linguistics: Human Language Technologies, NAACL-HLT 2019, Minneapolis, MN, USA, June 2-7, 2019, Volume 1 (Long and Short Papers)*, pages 4171–4186. Association for Computational Linguistics, 2019.
- [31] Tsung-Yi Lin, Piotr Dollár, Ross B. Girshick, Kaiming He, Bharath Hariharan, and Serge J. Belongie. Feature pyramid networks for object detection. In *2017 IEEE Conference on Computer Vision and Pattern Recognition, CVPR 2017, Honolulu, HI, USA, July 21-26, 2017*, pages 936–944. IEEE Computer Society, 2017.
- [32] Ethan Perez, Florian Strub, Harm de Vries, Vincent Dumoulin, and Aaron C. Courville. Film: Visual reasoning with a general conditioning layer. In Sheila A. McIlraith and Kilian Q. Weinberger, editors, *Proceedings of the Thirty-Second AAAI Conference on Artificial Intelligence*,

(AAAI-18), the 30th innovative Applications of Artificial Intelligence (IAAI-18), and the 8th AAAI Symposium on Educational Advances in Artificial Intelligence (EAAI-18), New Orleans, Louisiana, USA, February 2-7, 2018, pages 3942–3951. AAAI Press, 2018.

- [33] Fisher Yu and Vladlen Koltun. Multi-scale context aggregation by dilated convolutions. In Yoshua Bengio and Yann LeCun, editors, *4th International Conference on Learning Representations, ICLR 2016, San Juan, Puerto Rico, May 2-4, 2016, Conference Track Proceedings*, 2016.
- [34] Ronghang Hu, Marcus Rohrbach, Jacob Andreas, Trevor Darrell, and Kate Saenko. Modeling relationships in referential expressions with compositional modular networks. In *2017 IEEE Conference on Computer Vision and Pattern Recognition, CVPR 2017, Honolulu, HI, USA, July 21-26, 2017*, pages 4418–4427. IEEE Computer Society, 2017.
- [35] Hanwang Zhang, Yulei Niu, and Shih-Fu Chang. Grounding referring expressions in images by variational context. In *2018 IEEE Conference on Computer Vision and Pattern Recognition, CVPR 2018, Salt Lake City, UT, USA, June 18-22, 2018*, pages 4158–4166. Computer Vision Foundation / IEEE Computer Society, 2018.
- [36] Bohan Zhuang, Qi Wu, Chunhua Shen, Ian D. Reid, and Anton van den Hengel. Parallel attention: A unified framework for visual object discovery through dialogs and queries. In *2018 IEEE Conference on Computer Vision and Pattern Recognition, CVPR 2018, Salt Lake City, UT, USA, June 18-22, 2018*, pages 4252–4261. Computer Vision Foundation / IEEE Computer Society, 2018.
- [37] Licheng Yu, Hao Tan, Mohit Bansal, and Tamara L. Berg. A joint speaker-listener-reinforcer model for referring expressions. In *2017 IEEE Conference on Computer Vision and Pattern Recognition, CVPR 2017, Honolulu, HI, USA, July 21-26, 2017*, pages 3521–3529. IEEE Computer Society, 2017.
- [38] Licheng Yu, Zhe Lin, Xiaohui Shen, Jimei Yang, Xin Lu, Mohit Bansal, and Tamara L. Berg. Mattnet: Modular attention network for referring expression comprehension. In *2018 IEEE Conference on Computer Vision and Pattern Recognition, CVPR 2018, Salt Lake City, UT, USA, June 18-22, 2018*, pages 1307–1315. Computer Vision Foundation / IEEE Computer Society, 2018.
- [39] Xihui Liu, Zihao Wang, Jing Shao, Xiaogang Wang, and Hongsheng Li. Improving referring expression grounding with cross-modal attention-guided erasing. In *IEEE Conference on Computer Vision and Pattern Recognition, CVPR 2019, Long Beach, CA, USA, June 16-20, 2019*, pages 1950–1959. Computer Vision Foundation / IEEE, 2019.
- [40] Sahar Kazemzadeh, Vicente Ordonez, Mark Matten, and Tamara L. Berg. Referitgame: Referring to objects in photographs of natural scenes. In Alessandro Moschitti, Bo Pang, and Walter Daelemans, editors, *Proceedings of the 2014 Conference on Empirical Methods in Natural Language Processing, EMNLP 2014, October 25-29, 2014, Doha, Qatar, A meeting of SIGDAT, a Special Interest Group of the ACL*, pages 787–798. ACL, 2014.
- [41] Junhua Mao, Jonathan Huang, Alexander Toshev, Oana Camburu, Alan L. Yuille, and Kevin Murphy. Generation and comprehension of unambiguous object descriptions. In *2016 IEEE Conference on Computer Vision and Pattern Recognition, CVPR 2016, Las Vegas, NV, USA, June 27-30, 2016*, pages 11–20. IEEE Computer Society, 2016.
- [42] Hugo Jair Escalante, Carlos A. Hernández, Jesús A. González, Aurelio López-López, Manuel Montes-y-Gómez, Eduardo F. Morales, Luis Enrique Sucar, Luis Villaseñor Pineda, and Michael Grubinger. The segmented and annotated IAPR TC-12 benchmark. *Comput. Vis. Image Underst.*, 114(4):419–428, 2010.
- [43] Tsung-Yi Lin, Michael Maire, Serge J. Belongie, James Hays, Pietro Perona, Deva Ramanan, Piotr Dollár, and C. Lawrence Zitnick. Microsoft COCO: common objects in context. In David J. Fleet, Tomás Pajdla, Bernt Schiele, and Tinne Tuytelaars, editors, *Computer Vision - ECCV 2014 - 13th European Conference, Zurich, Switzerland, September 6-12, 2014, Proceedings, Part V*, volume 8693 of *Lecture Notes in Computer Science*, pages 740–755. Springer, 2014.
- [44] Thomas Wolf, Lysandre Debut, Victor Sanh, Julien Chaumond, Clement Delangue, Anthony Moi, Pierrick Cistac, Tim Rault, Rémi Louf, Morgan Funtowicz, and Jamie Brew. Huggingface’s transformers: State-of-the-art natural language processing. *CoRR*, abs/1910.03771, 2019.

- [45] Diederik P Kingma and Jimmy Ba. Adam: A method for stochastic optimization. *arXiv preprint arXiv:1412.6980*, 2014.
- [46] Ilya Loshchilov and Frank Hutter. SGDR: stochastic gradient descent with warm restarts. In *5th International Conference on Learning Representations, ICLR 2017, Toulon, France, April 24-26, 2017, Conference Track Proceedings*. OpenReview.net, 2017.
- [47] Liwei Wang, Yin Li, Jing Huang, and Svetlana Lazebnik. Learning two-branch neural networks for image-text matching tasks. *IEEE Trans. Pattern Anal. Mach. Intell.*, 41(2):394–407, 2019.
- [48] Bryan A. Plummer, Paige Kordas, M. Hadi Kiapour, Shuai Zheng, Robinson Piramuthu, and Svetlana Lazebnik. Conditional image-text embedding networks. In Vittorio Ferrari, Martial Hebert, Cristian Sminchisescu, and Yair Weiss, editors, *Computer Vision - ECCV 2018 - 15th European Conference, Munich, Germany, September 8-14, 2018, Proceedings, Part XII*, volume 11216 of *Lecture Notes in Computer Science*, pages 258–274. Springer, 2018.
- [49] Arka Sadhu, Kan Chen, and Ram Nevatia. Zero-shot grounding of objects from natural language queries. In *2019 IEEE/CVF International Conference on Computer Vision, ICCV 2019, Seoul, Korea (South), October 27 - November 2, 2019*, pages 4693–4702. IEEE, 2019.